Monthly Notices
of the
ROYAL ASTRONOMICAL SOCIETY

Mon. Not. R. Astron. Soc. **402,** 1213–1220 (2010) doi:10.1111/j.1365-2966.2009.15958.x

An anomalous *Wilkinson Microwave Anisotropy Probe* signal in the ecliptic plane

J. M. Diego,[1⋆] M. Cruz,[2] J. González-Nuevo,[3] M. Maris,[4] Y. Ascasibar[5] and C. Burigana[6]

[1]*IFCA, Instituto de Física de Cantabria (UC-CSIC) Avda. Los Castros s/n, 39005 Santander, Spain*
[2]*Departamento de Matemáticas, Estadística y Computación, Universidad de Cantabria. Avda. Los Castros s/n, 39005 Santander, Spain*
[3]*SISSA-ISAS, via Beirut 4, I-34014 Trieste, Italy*
[4]*INAF–Osservatorio Astronomico Trieste, Via G.B.Tiepolo 11, I34100 Trieste, Italy*
[5]*Universidad Autónoma de Madrid, Departamento de Fisica Teorica, Madrid E-28049, Spain*
[6]*INAF–IASF Bologna, via Gobetti 101, I-40129 Bologna, Italy*

Accepted 2009 October 28. Received 2009 September 15; in original form 2009 February 25

ABSTRACT

We report the detection of a high Galactic latitude, large-scale, 7σ signal in *Wilkinson Microwave Anisotropy Probe* (*WMAP*) 5-year data and spatially correlated with the ecliptic plane. Two possible candidates are studied, namely unresolved sources and Zodiacal light emission. We determine the strength of the Zodiacal light emission at *WMAP* frequencies and estimate the contribution from unresolved extragalactic sources. Neither the standard Zodiacal light emission nor the unresolved sources alone seem to be able to explain the observed signal. Other possible interpretations such as Galactic foregrounds and diffuse Sunyaev–Zel'dovich effect also seem unlikely. We check if our findings could affect the low-ℓ anomalies which have been reported in the *WMAP* data. Neither Zodiacal light emission nor unresolved point-source residuals seem to affect significantly the quadrupole and octupole measurements. However, a signal with a quasi-blackbody spectrum and with a spatial distribution similar to the Zodiacal light emission could explain both the anomalous signal and the low-ℓ anomalies. Future data (*Planck*) will be needed in order to explain the origin of this signal.

Key words: Galaxy: general – cosmic microwave background – infrared: Solar system.

1 INTRODUCTION

Data from the *Wilkinson Microwave Anisotropy Probe* (*WMAP*) (see Hinshaw et al. 2008 for a summary of the 5-year data release) revealed a wealth of information not only about the cosmological model but also about our own Galaxy. The simplest model describing the *WMAP* observations is comprised of the cosmic microwave background (CMB), extragalactic point sources (PS), Galactic components (synchrotron radiation, dust and free–free emission) all of them convolved with optical beams, and anisotropic instrumental noise. A combination of these six components provides a good description of the observations in different channels over a relatively wide range of frequencies ($30 < \nu < 90$ GHz). Some controversy arose when anomalous residual signals appeared once the templates accounting for the components (with the exception of the noise for which no template can be produced) were subtracted from the original data (Finkbeiner 2004; Dobler & Finkbeiner 2008). Detecting such residuals is not surprising (especially near the Galactic plane) since the spectral index is expected to vary across the sky for most of the components. These anomalous residual signals (or *anomalies*) could be the reason for the unusually low-CMB quadrupole or for the alignment between octupole and quadrupole (another unusual feature; de Oliveira-Costa & Tegmark 2006; Copi et al. 2006; Land & Magueijo 2007). In Abramo, Sodré & Wuensche (2006), the authors study the existence of an hypothetical foreground which could explain the two mentioned anomalies (low amplitude of the quadrupole and alignment). They showed how the anomalies could be explained as due to foreground residuals extending over an area of $\approx$0.5 sterad, with a peak amplitude of about 20 μK, an rms average of 8 μK and located in the ecliptic plane. Bunn & Bourdon (2008) argue against this possibility. They maintain that contaminants in the CMB cannot explain the lack of power of the low-ℓ multipoles. Instead, this lack of power can be used as '*a strong argument against the existence of undiagnosed foreground contamination*'. The authors of this last work, though, consider that the possible contaminant is uncorrelated with the primordial CMB signal. This, of course, would not be the case of a signal which is aligned with the ecliptic and hence strongly correlated with the measured quadrupole and octupole in *WMAP*.

⋆E-mail: jdiego@ifca.unican.es

Here, we present the detection of a new anomaly detected in *WMAP* 5-year data which appears at high Galactic latitudes and which resembles the description given in Abramo et al. (2006). This anomaly was first reported in Diego & Ascasibar (2008) using *WMAP* 3-year data. We attempt to explain it as due to a combination of several components which have not been accounted for in previous works, the Zodiacal light emission (ZLE) and the contribution from unresolved sources [these are also called PS]. The ZLE has been detected with a high significance at higher frequencies by experiments like the *Infrared Astronomical Satellite* (*IRAS*; Jones & Rowan-Robinson 1993) or the Diffuse Infrared Background Experiment (DIRBE; Hauser et al. 1997). Extrapolations from these observations down to *WMAP* frequencies predict a weak signal, below the instrumental noise sensitivity at all scales (Maris, Burigana & Fogliani 2006). The predictions are made assuming that the dust has a single component and the spectral frequency dependence of the intensity of the emission behaves as a blackbody with a temperature of $T \approx 240$ K modified by a factor λ^{-2} at wavelengths $\lambda > 150$ μm (Fixsen & Dwek 2002). However, multiple dust grain sizes are expected in the zodiacal cloud so one would expect deviations from the λ^{-2} law. In this paper, we show how modifications of the λ^{-2} law can result in a signal which could be detected in the *WMAP* data. Analysing *WMAP* data, we find a signal which approximately correlates spatially with the ZLE and with a dust-like spectrum. We also consider other possible signals which could produce a large-scale signal like the one observed in *WMAP*. One of these possibilities is microwave emission due to unresolved (or point) sources. Finally, we discuss the implications of this signal for aspects such as the measurements of the quadrupole and octupole in *WMAP* 5-year data.

2 *WMAP* LARGE-SCALE RESIDUALS

As a first (and good) approximation, *WMAP* data can be decomposed into six components, namely CMB, resolved PS and the three Galactic components (synchrotron, dust and free–free), and the residual is assumed to be the contribution from instrumental noise. This simple decomposition manages to reproduce the observations with high accuracy. Nevertheless, one should expect other components to contribute as well to the *WMAP* observations. One of these components is the unresolved population of extragalactic sources. Only the brightest sources (a few hundreds) are masked out in the *WMAP* data. Many unresolved sources (PS) still contribute to the data. This contribution can be particularly important if the PS are correlated. For radio-selected extragalactic sources, their clustering introduces generally a small contribution to the temperature fluctuations (Dunlop & Peacock 1990; Blake & Wall 2002; González-Nuevo, Toffolatti & Argüeso 2005). In the case of the infrared sources, low-z galaxies dominate the counts at bright flux levels (Negrello et al. 2007) (i.e. the kind of sources detected by the *IRAS*; Beichman et al. 1988). Due to the inhomogeneous distribution of matter in the local Universe, we expect overdensities in the flux distribution produced by the infrared sources. One can imagine that a diffuse component could be contributing to the data at scales similar to the correlation scale of the infrared sources. Such a signal would be easier to see once the small scales are filtered out. We use *WMAP* data to look for possible large-scale residuals. Combining the different frequency channels and using Galactic foreground templates, we can minimize the contribution from our Galaxy and the CMB itself. Filtering out the smaller scales, the instrumental noise contribution is reduced while the large-scale residuals are highlighted.

By residuals we mean components which are not considered in the cleaning process of *WMAP* 5-year data. The *WMAP* team provided foreground-reduced maps where Galactic synchrotron, free–free and dust templates are subtracted from the data. We use these *clean* maps and remove the CMB component by combining the Q (at 41 GHz), V (at 61 GHz) and W (at 94 GHz) frequency maps. In particular, we choose the combination $V + W - 2Q$ following Diego & Ascasibar (2008) where these authors found an excess signal around the Virgo region in the combination $V + W - 2Q$. This combination maximizes the signals with a spectral dependence similar to the Sunyaev–Zel'dovich effect, infrared and/or synchrotron. There are other possible combinations which remove the primary CMB. This CMB free combination should contain mainly noise. In a combination like this one, signals like dust emission or the thermal Sunyaev–Zel'dovich effect will appear as warm positive fluctuations while signals due to synchrotron radiation will appear as colder negative fluctuations. The combination also $V + W - 2Q$ attempts to maximize the frequency variation between the different channels. Other combinations involving differences like $W - V$ would be closer in frequency and hence less sensitive to non-blackbody signals. Before combining the maps, they are degraded to the resolution of the Q band. We also subtract the monopole and dipole in the combined map to account for possible calibration differences between the channels. The final map is then smoothed with a 7° Gaussian kernel to reduce the instrumental noise contribution. The result is presented in Fig. 1 in Galactic coordinates (and in Fig. 2 in ecliptic coordinates). The map shows two very red regions (i.e. with a dust-like spectrum) in the north-east and south-west quadrants. The central band with zero values is due to the exclusion mask used in the analysis. This mask also excludes the brightest PS in *WMAP* data. On the other side, blue regions indicate areas with

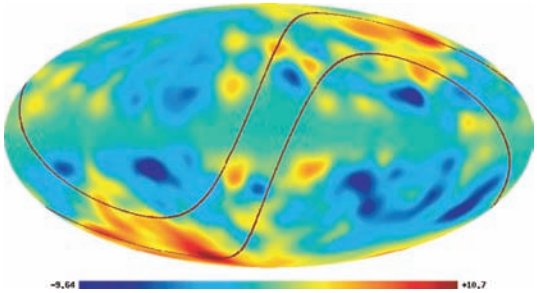

Figure 1. 7° smoothed *WMAP* residual of the combination $V + W - 2Q$. The colour bar units are given in μK. The two curved lines show the ecliptic plane (±15°). The Galactic Centre is at the centre of the image. Galactic longitude increases to the left.

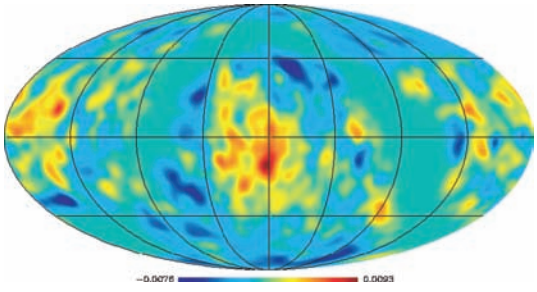

Figure 2. Same as Fig. 1 but with a 10° smoothing kernel and in ecliptical coordinates. The units are mK and the grid spacing is 45°. The Galactic Centre is about 90° to the right of the centre of the image (and about zero latitude).

a possible synchrotron-like spectrum. The blue regions concentrate near the Galactic plane indicating that there might still be a residual Galactic synchrotron component in the combination map $V + W - 2Q$. This has been observed before (Bennett et al. 2003; Finkbeiner 2004). There is also a blue region near the Magellanic clouds indicating a possible contribution from spatially correlated radio PS in this area.

This paper will focus in the redder regions and will assume that the bluer regions are of Galactic origin. The Galactic interpretation for the redder regions is less likely due to their high latitudes. By looking at the individual differences (Fig. 3), we note that the redder regions appear in the three individual differences. In particular, the south-west redder region shows a clear pattern which is seen in the three differences. By looking at the intensity of the peak in this region (circles in Fig. 3), we can infer the spectral index of the region. The *WMAP* intensity in the circled area is shown as diamonds in Fig. 4. We compare this intensity with two models. The first one, represented by the plus symbol, is a signal with an intensity of 4 KJy sr^{-1} in the V band and a emissivity law of ν^2 (very similar to a blackbody law in the Rayleigh–Jeans region) in the V band. The second one, represented by a triangle symbol, is a signal with an emissivity law ν^4 and intensity 0.35 KJy sr^{-1} (this model would correspond to thermal dust emission). The physical interpretation of the second model could be for instance a population of infrared sources with an overdensity of 0.35 KJy sr^{-1} in these regions. Since the redder regions approximately correlate with the ecliptic plane (which also has a modified blackbody spectrum), it is tempting to think that the redder zones could be due to ZLE from the ecliptic plane. It is also tempting to interpret the redder zones as due to a higher concentration of infrared extragalactic sources in these regions. But, before we explore these two possibilities we should focus on another possible explanation. As the redder regions appear

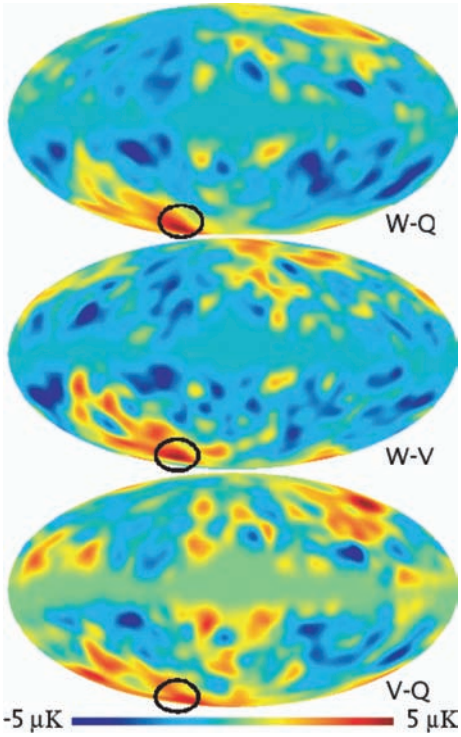

Figure 3. Differences after smoothing with a 7° Gaussian in the three individual difference maps. The circle marks the spot where the amplitude is measured in Fig. 4.

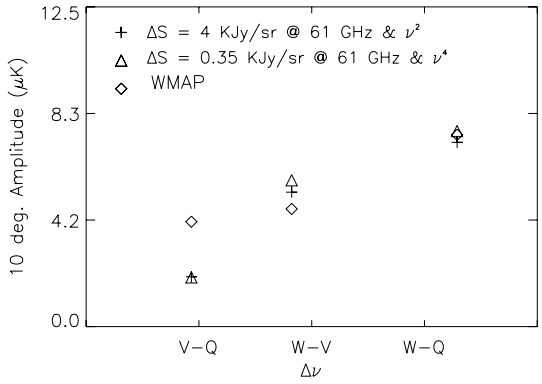

Figure 4. Amplitude at the positions marked in Fig. 3 and for two different models. The diamond symbol marks the amplitudes of the *WMAP* signal. The plus symbol corresponds to a model with an overdensity in flux of 4 KJy sr^{-1} (at 61 GHz) and with a emissivity law of ν^2 (almost like a blackbody). The triangle is for a different model with an overflux density of 0.35 KJy sr^{-1} and a emissivity law, ν^4 (typical of thermal dust emission).

in areas of the sky where the instrumental noise is higher than the average, they could be just fluctuations of the noisy background in the combined map $V + W - 2Q$. Whether the red regions are consistent or not with the instrumental noise is something we address in the next section.

3 STATISTICAL SIGNIFICANCE

To address the significance of the redder zones in the Northern and Southern hemispheres, we perform 200 simulations of the instrumental noise. The noise in the $V + W - 2Q$ map was simulated using the number of observations per pixel and per band given by the *WMAP* team and the instrument sensitivity. Independent noise maps were made for each one of the individual channels and those were combined in the way described in the previous section [i.e. they are degraded to the resolution of the Q map, combined and filtered with a Gaussian of full width at half-maximum (FWHM) 7°]. We checked that $1/f$ noise is not an issue by using the noise simulations from the first-year *WMAP* data (which include $1/f$ noise) and verified that no significant structures appeared on large scales due to $1/f$ noise. We look at the maxima of the combined simulated noise maps and compare them with the observed value of $\approx 10.7 \times 10^{-3}$ mK. The result is shown in Fig. 5. We made histograms similar to the one shown in Fig. 5 but for the individual differences ($W - V$, $W - Q$ and $V - Q$) and found similar results. The largest deviation was found in $W - Q$ (maximum of data at 7.5 μK compared with maximum of simulations at 3.5 μK) followed by $V - Q$ (maximum of data at 4.5 μK compared with maximum of simulations at 2.9 μK). The difference $W - V$ has a maximum in the data at 4.6 μK which should be compared with a maximum in the simulations at 4 μK, (i.e. marginally consistent with the noise hypothesis). The redder zones in the $V + W - 2Q$ *WMAP* data are approximately a 7σ fluctuation with respect to the expected fluctuations of the instrumental noise. Hence, simulations show that the redder structures seen in the Northern and Southern hemispheres are not compatible with fluctuations of the instrumental noise and therefore they must be caused by a real signal. Some structures are visible in all the difference maps ($W - V$, $V - Q$ and $W - Q$). For instance, near the south Galactic pole and to the west, the red structure can be seen in all the difference maps (see Fig. 3) suggesting that this is a real high-latitude feature and neither a large-scale fluctuation of the instrumental noise nor a systematic effect. In the next sections, we

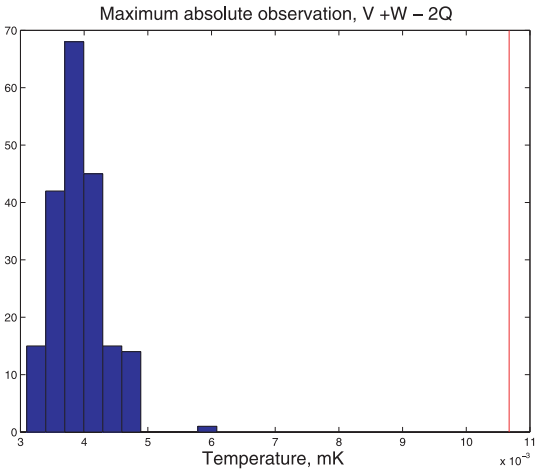

Figure 5. Histogram of the maximum of 200 simulated $V + W - 2Q$ noise maps (on a 7° scale). The vertical line between 10 and 12 μK is the actual observed value.

will explore some of the possible explanations for the residuals. We will consider two possible components which combined with the instrumental noise might explain the observations. The first one is the ZLE, already detected at higher frequencies by DIRBE (Hauser et al. 1997) and *IRAS* (Jones & Rowan-Robinson 1993). The second one is the contribution from spatially correlated infrared sources. One extra possibility (the Sunyaev–Zel'dovich effect; Sunyaev & Zel'dovich 1972) was already explored in a previous paper (Diego & Ascasibar 2008) finding that the Sunyaev–Zel'dovich effect was an unlikely explanation.

4 ZODIACAL LIGHT EMISSION

Dust grains in the ecliptic plane emit thermal radiation. Averaging this signal over one orbital year, we can see a pattern which follows the ecliptic plane. This pattern is shown in Fig. 6. This radiation is known as the ZLE and it is mainly seen in the infrared through thermal emission of the dust particles. In the optical, the same dust particles scatter the light of the sun making it detectable as well at this wavelengths. The figure shows how the plane with the maxima of ZLE crosses the redder regions in the *WMAP* data. However, the centre of the redder zones does not coincide with the maximum of the ZLE. At sub-mm frequencies the ZLE was observed by DIRBE and *IRAS*. For our purposes, we will follow Kelsall et al. (1998) to perform the simulation of the ZLE. The simulation was made at 240 μm using the code written by B.A Franz which implements the model described in Kelsall et al. (1998). In that work, the authors

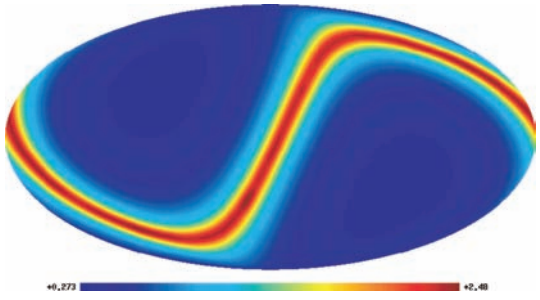

Figure 6. 1 year average of the ZLE at 240 μm in Galactic coordinates. The map has been filtered with a 7° Gaussian for presentation purposes. The colour table shows the units in MJy sr^{-1}.

assumed multiple components for the dust density distribution: a smooth cloud; three asteroidal dust bands and a circumsolar ring near 1 au. This model manages to describe well the ZLE observed by DIRBE from 1.25 to 240 μm. We extrapolated this signal down to *WMAP* frequencies using the following law:

$$Z_i = F_i Z_{240}, \tag{1}$$

where Z_i is the intensity of the ZLE in the *WMAP* band i (i stands for the $\nu = 41$ GHz or Q band, $\nu = 61$ GHz or V band and $\nu = 94$ GHz or W band), and F_i accounts for the frequency dependence of the ZLE. Z_{240} is the template of ZLE as predicted by the code described above at 240 μm (and given in MJy sr^{-1} units). The ZLE map at 240 μm was pixelized using HEALPIX (Gorski et al. 2005[1]) and transformed into Galactic coordinates. For the frequency dependence, we assumed the following law:

$$F_i = g_i \left(\frac{B_i}{B_{240}}\right)\left[\frac{240\,\mu\mathrm{m}}{\lambda_i\,(\mu\mathrm{m})}\right]^{\alpha} \mu\mathrm{K\,MJy^{-1}\,sr}, \tag{2}$$

where $\lambda_i = 3 \times 10^5/\nu_i(\mathrm{GHz})$ in μm [ν_i is either 41 (Q), 61 (V) or 94 (W) GHz] and B_i is the blackbody emissivity law and for $T = 240K$ (with B_{240} the corresponding emissivity at 240 μm). The factor g_i accounts for the conversion from MJy sr^{-1} to μK ($g_Q = 20.2 \times 10^3$, $g_V = 9.62 \times 10^3$ and $g_W = 4.6 \times 10^3$ all in μK (MJy^{-1} sr^{-2}) units. When combining the different frequency maps, a combined F factor can be defined as follows:

$$F_{\mathrm{comb}} = F_V + F_W - 2F_Q\ \mu\mathrm{K\,MJy^{-1}\,sr}. \tag{3}$$

Hence, the intensity of the ZLE (in μK units) in the combination $V + W - 2Q$ can be easily computed from the template Z_{240} (shown in Fig. 6) as

$$Z_{\mathrm{comb}} = F_{\mathrm{comb}} Z_{240}\ \mu\mathrm{K}. \tag{4}$$

The ZLE light behaves like a grey body at wavelengths shorter than 150 μm but at longer wavelengths it falls off more quickly. The fall off can be computed as a ν^{α} correction to the blackbody spectrum. In Fixsen & Dwek (2002), α was found to be around 2 in the submillimetre to millimetre region, but the error bars allow a range of α especially at longer wavelengths. A value of $\alpha = 2$ corresponds to emission dominated by a population of dust grains with a narrow range of sizes. A deviation from the $\alpha = 2$ exponent is expected when the interplanetary dust cloud is filled with grains of different sizes. The value of α affects the amplitude of the predicted ZLE signal. We show this in Fig. 7 where the factor F_{comb} is computed for different values of α. From fig. 2 in Fixsen & Dwek (2002), a valid range for α would be $1.5 < \alpha < 2.5$ for wavelengths shorter than 1000 μm. It is unclear how the ZLE light behaves at $\lambda > 1000$ μm and one could possibly think of effective α smaller than 1.5 (see Fig. 7). Small values of α at wavlengths $\lambda > 1000$ μ m are expected if there is a significant amount of a yet undetected cold dust component with grain sizes larger than the ones responsible for the emission detected by *IRAS* and/or DIRBE. In this work, we will consider the case (consistent with the results of Fixsen & Dwek 2002) where $\alpha = 1.5$, bearing in mind that smaller α at *WMAP* frequencies cannot be ruled out by current data. Extrapolating the predicted ZLE intensity from 240 μm to the *WMAP* frequencies with the value of α assumed above, we predict an intensity for the Zodiacal signal in the combined $V + W - 2Q$ which is significantly smaller than the intensity of the redder zones in the Northern and Southern hemispheres in the $V + W - 2Q$ difference

[1] available at http://healpix.jpl.nasa.gov/

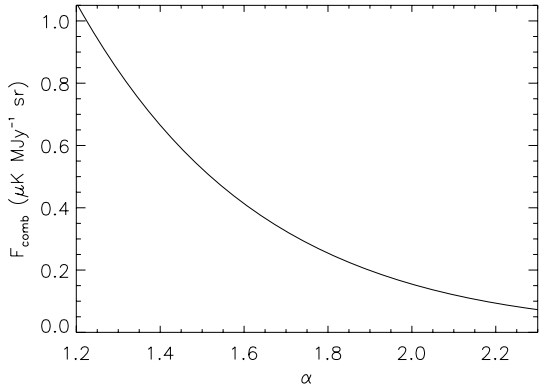

Figure 7. Dependency of the conversion factor ($F_{\rm comb}$) with the exponent α.

maps. We predict a maximum amplitude for the ZLE of $\sim$1 μK in $V + W - 2Q$ after filtering with a 7° Gaussian which should be compared with the $\sim$10 μK amplitude observed in *WMAP* data. This can also be seen by combining Figs 6 and 7. In Fig. 6, the maximum amplitude is 2.4 MJy sr^{-1} at 240 μm which multiplied for the corresponding $F_{\rm comb} \approx 0.5$ ($\alpha = 1.5$ in Fig. 7) renders a maximum amplitude of $\sim$1 μK. From Fig. 7, we see that if $\alpha \sim 1$ the contribution from the ZLE becomes more important, but is still far from the required 10 μK. Hence, we can conclude that it seems unlikely that the redder zones are due to standard ZLE emission.

5 UNRESOLVED SOURCES

Another possible source of contamination in the *WMAP* data is the emission from unresolved extragalactic (or even compact Galactic) sources. In general terms, we will refer to these sources as unresolved source or PS. *WMAP* masks out the brightest sources but this removes only a few hundred sources above 0.5 Jy. Many other bright sources remain in the data. On small scales (arcminute), the signal coming from these sources can be comparable to the CMB in terms of power spectrum amplitude. On larger scales (degrees), the amplitude of the power spectrum due to PS is negligible compared to the CMB power spectrum. However, a combination map like the one used in this work ($V + W - 2Q$) removes the primary CMB background leaving the PS as a possible significant contribution to the residuals (especially if the PS are clustered). The contribution coming from extragalactic sources might increase their integrated signal in certain regions over scales of many degrees if these sources are clustered. The most significant contribution is expected to come from nearby extragalactic clustered sources. At large distances, the clustering scale of the sources is under a few degrees (where the CMB clearly dominates) and the distribution of sources is also more homogeneous over the sky. The *IRAS* all sky map, for instance, is a good tracer for the possible contribution of nearby clustered infrared sources. We perform an all-sky simulation at *WMAP* frequencies of the PS under 0.5 Jy using the same procedure that in the Planck Sky Model (PSM; Leach et al. 2008) to extrapolate their fluxes from the available observational catalogues. In the case of radio sources, we have used the Green Bank 4.85 GHz northern sky survey (GB6, Gregory et al. 1996) and the Parkes-MIT-NRAO at 4.85 GHz (PMN; Gregory et al. 1994) catalogues. The holes of these two surveys are filled with the NRAO VLA (Very Large Array) Sky Survey at 1.4 GHz (NVSS, Condon et al. 1998) and the Sydney University Molonglo Sky Survey (SUMSS) at 0.84 GHz (Mauch et al. 2003). The cross-correlation of catalogues at different frequencies has been carried out degrading the higher resolution map to the resolution of the lower resolution one. In practice, whenever the higher resolution (NVSS or SUMSS) catalogue contains more than one source within the resolution element of the lower resolution (4.85 GHz) one, we have summed the NVSS or SUMSS fluxes, weighted with a Gaussian response function centred on the nominal position of the 4.85 GHz source and with the FWHM equal to the resolution of the 4.85 GHz survey. To correct for the contributions of background sources, we have subtracted the average flux of a set of control fields, free of 4.85 GHz sources, from the summed NVSS or SUMSS fluxes associated with 4.85 GHz sources. In this way, we obtained spectral indices from $\sim$1 to $\sim$5 GHz for a complete sample of sources over about 95 per cent of the sky to a flux limit of $\sim$50 mJy. To avoid very extreme values, we have changed the spectral indexes of the outliers of the distribution (sources with spectral indexes that differ more than three times the standard deviation from the median value of the distribution) to the median value. Additionally, for those sources at $\sim$5 GHz without an spectral index we have randomly assigned them one from the observed distribution. Finally, in the case of sources observed only at lower frequency, we have repeated the same procedure but using a Gaussian distribution based on the observational results of Fomalont et al. (1991) [$\langle\alpha\rangle = 0.8$ and $\sigma(\alpha) = 0.3$].

By observing the southern extragalactic sources of the Khur sample (Kühr et al. 1981; Stickel, Meisenheimer & Kuehr 1994) with the Australia Telescope Compact Array, Ricci et al. (2006) found evidences of an spectral steepening between 5 and 20 GHz [steep sources ($\alpha > 0.5$; $S_\nu \propto \nu^{-\alpha}$): $\langle\Delta\alpha\rangle = 0.47$ and $\sigma(\Delta\alpha) = 0.3$; flat sources ($\alpha < 0.5$): $\langle\Delta\alpha\rangle = 0.24$ and $\sigma(\Delta\alpha) = 0.3$]. For this reason, to extrapolate the fluxes of our sample from 5 to 20 GHz we have introduced a random spectral index steepening based on these results (the observed distribution was approximated as a Gaussian).

Due to the complex spectral shape of radio sources, the power-law approximation holds only for a limited frequency range. To extrapolate the fluxes to still higher frequencies, we used the multifrequency *WMAP* data (Bennett et al. 2003; New Extragalactic *WMAP* Point Source (NEWPS), López-Caniego et al. 2007) to derive the distribution of differences between spectral indices above and below 20 GHz. Such distribution can be approximated by a Gaussian with mean 0.29 and dispersion 0.43. To each source, we have associated a spectral index change drawn at random from the distribution. This extrapolation method has been tested by comparing the number counts calculated from the extrapolated catalogue with data from different surveys and with model predictions (Massardi et al. 2008).

For the infrared side, a compilation including all far-infrared sources taken from the *IRAS* catalogue (Beichman et al. 1988), point source catalogue (PSC) and faint source catalogue (FSC; Moshir et al. 1992) was made available to the Planck collaboration by Dave Clements.[2] The FSC catalogue is restricted to regions away from the Galactic plane (Galactic latitudes larger than 10°) and the PSC catalogue avoids regions with high confusion noise, mostly in the Galactic plane. Hence, the final source density is a function of Galactic latitude (this issue should not be a problem for our studies at high latitude).

For the thermal sources, it is assumed that they have a spectral energy distribution (SED) given by a modified blackbody law [$\nu^b B(\nu, T)$]. The SED is used to extrapolate or predict the fluxes at frequencies not observed by *IRAS*. When a source is detected at

[2] http://astro.ic.ac.uk/∼dlc/input_cat.html

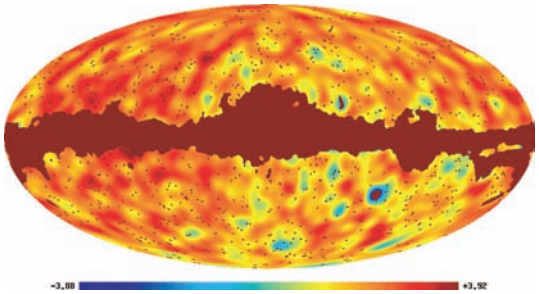

Figure 8. Predicted contribution from PS with fluxes below 0.5 Jy in $V + W - 2Q$ and in μK. The *WMAP* mask is shown as well. Note the negative contribution around the Magellanic cloud.

only one *IRAS* frequency, the parameters b and T are taken from the average SED derived from the Submilimeter Local Universe Galaxy Survey (Dunne et al. 2000). They correspond to $b = 1.3$, $T = 35$ K. If the source is detected at 60 and 100 μm, the value $b = 1.3$ is still maintained but the temperature can be derived from the modified blackbody law. The normalization of the flux is derived from the *IRAS* data. The non-thermal component is removed before SED fitting. In this way, we obtained a source catalogue that looks approximately complete down to ∼80 mJy at 857 GHz and can be easily extrapolated down to *WMAP* frequencies.

In Fig. 8, we show the predicted contribution from PS in the $V + W - 2Q$ map including only sources with fluxes below 0.5 Jy at each frequency (Q, V or W). The PS contribution is filtered with a 7° Gaussian and the result shows fluctuations of the order of a few μK in $V + W - 2Q$, but still far away from the observed 10 μK level. Given our model, the combination of ZLE, PS and instrumental noise could roughly explain half the amplitude of the observed signal in *WMAP* data.

6 OTHER CANDIDATES. GALACTIC EMISSION AND SUNYAEV–ZEL'DOVICH EFFECT

Whatever the cause of the redder zones is, we know that it must have a ν^α spectrum with $\alpha \geq 2$. There are two other candidates, namely thermal dust emission from the Galaxy and the Sunyaev–Zel'dovich effect, that fulfil this condition. The possibility that the redder zones are due to thermal dust is unlikely since the two red regions are close to the Galactic poles (where the dust emission is minimal). Nevertheless, they could be explained if the cleaning process removed more dust than needed, leaving the northern and southern Galactic poles with a positive relative signal when computing the individual differences of the *WMAP* channels. In this scenario, a negative temperature difference would be expected near the Galactic plane (without the mask), but a small positive value is observed, suggesting that the dust template has not been oversubtracted. The other possibility is a diffuse Sunyaev–Zel'dovich effect coming from distant massive structures. Even though the Sunyaev–Zel'dovich effect produces a decrement in each of the individual temperature maps, it yields a positive signal in all three differences $V - Q$, $W - V$ and $W - Q$. Combining X-ray and *WMAP* 3-year data, it has recently been shown (Diego & Ascasibar 2008) that the Virgo region, near the redder zone in the north, can contribute with a maximum of about 5 μK when filtered with a 7° Gaussian, falling quickly at angular distances of a few degrees from the centre of the cluster. A very extended (9 Mpc) warm–hot intergalactic medium cloud around Virgo would contribute about an extra 1 μK. The Virgo region could thus explain *part* of the observed signal in the northern red zone, but not the one located in the south. More generally, very massive and distant structures with a hot and extended gas component (e.g. clusters and large-scale filaments) are constrained by their X-ray emission (see e.g. Diego et al. 2002). Assuming a standard β profile for the gas density and a temperature of 3 keV, any model explaining the red zones in the residual map would exceed the diffuse X-ray emission observed by *ROSAT*. We then conclude that, although the Sunyaev–Zel'dovich effect may contribute to the observed signal, it is unlikely that it is the dominant physical process behind it.

7 IMPLICATIONS FOR THE MEASURED QUADRUPOLE AND OCTUPOLE OF THE CMB

If a combination of the ZLE and extragalactic PS are affecting the *WMAP* data on large scales, it is possible that it will affect the measurements of the low multipoles. This possibility is even more realistic if we realize that the low multipoles seem to be aligned in a direction which follows the ecliptic (Copi et al. 2006; de Oliveira-Costa & Tegmark 2006; Land & Magueijo 2007). So far, we have considered only the signals in the $V + W - 2Q$ combination maps. In order to assess how much of this signal is affecting the CMB, a first-order approximation would be to take the equivalent of the internal linear combination but for the signal considered at the three *WMAP* frequencies. The best CMB map (or internal linear combination) was extracted by the *WMAP* team by combining the different bands with some optimal weights that reduce the foregrounds while keeping the CMB signal (see e.g. Bennett et al. 2003 where the authors show how the internal linear combination is mostly dominated by the data in the V band). For our purposes, we will assume the weights derived by Bennett et al. (2003). Our internal linear combination will be then $1.591 \times V + 0.052 \times Q - 0.079 \times W$. By looking at the quadrupole and octupoles of the simulated ZLE (assuming $\alpha = 1.5$) plus PS (with fluxes less than 0.5 Jy), we find that the quadrupole has very little power (amplitude less than 1 μK or about 3 per cent of the measured amplitude from *WMAP* data). A similar situation is observed when we compare the measured octupole and the octupole due to the contribution from the ZLE and PS. Regarding the possible contribution from the Sunyaev–Zel'dovich effect in the Virgo region, as noted by Dolag et al. (2005), the contribution from Virgo (and other nearby structures) is far too small to affect significantly the measurements of the quadrupole and octupole.

Even though our models cannot explain the excess in $V + W - 2Q$, the excess is real and it must be caused by some real signal. To test the possible impact on the quadrupole and/or octupole, we consider two toy models. In the first toy model, it is interesting to speculate about the possibility that such a signal is proportional to the ZLE (or another signal concentrated around the ecliptic plane). For the signal to be a significant contribution to the quadrupole, it should have a different frequency dependence that the one assumed above ($\alpha = 2$). Instead, we will consider a semi-blackbody spectrum ($\alpha = 0$). The physical interpretation for this signal could be for instance a very cold dust in quasi-thermal equilibrium. This has not been observed and its existence is at this moment pure speculation. However, such a signal could potentially explain the low amplitude of the quadrupole and may be the unusual alignment with the octupole. To test this, we assume this hypothetical model to have the spatial distribution of the ZLE (see Fig. 6). We model the frequency dependence of this signal as ν^2, i.e. very similar to a blackbody, and choose its normalization such that its amplitude

is approximately 10 μK in $V + W - 2Q$ band (after filtering with a 7° Gaussian). This signal would explain the magnitude of the redder zones observed by *WMAP* although it does not explain the lack of signal in some regions in the ecliptic plane. Since the signal behaves almost like a blackbody, it would be difficult to detect in the component separation process and it would be confused as a CMB signal. With this toy model, we compute the contribution to the internal linear combination using the same weights as above ($1.591 \times V + 0.052 \times Q - 0.079 \times W$). The final map has a maximum amplitude of about 40 μK when filtered with a 7° Gaussian which is well below the maximum of the internal linear combination map for the CMB (range $\sim \pm 130$ μK) when filtered with the same scale. We can now derive the quadrupole and octupole of this map and compare with the observed values. We find that the quadrupole has significant power and is anticorrelated with the measured quadrupole in *WMAP* 5-year data (see Fig. 9). This anticorrelation would explain why the quadrupole has an unusually low amplitude (Hinshaw et al. 1996; Bennett et al. 2003) as this hypothetical signal is suppressing a significant amount of the power. In Fig. 9, we show how the CMB quadrupole would look like if the contribution from this signal is subtracted from the measured quadrupole in the Internal Linear Combination (ILC) map. We see how the amplitude of the CMB quadrupole increases nearly a factor of 2. Regarding the octupole, we found that a signal like this contributes with a negligible amplitude (≈1 μK). We also found that only even multipoles have a significant amplitude and affect the measured power of the CMB while the effect from the odd multipoles (like the octupole) can be neglected. The anomalous signal modifies slightly the direction of the quadrupole and could perhaps explain the anomalous quadrupole–octupole alignment. Our

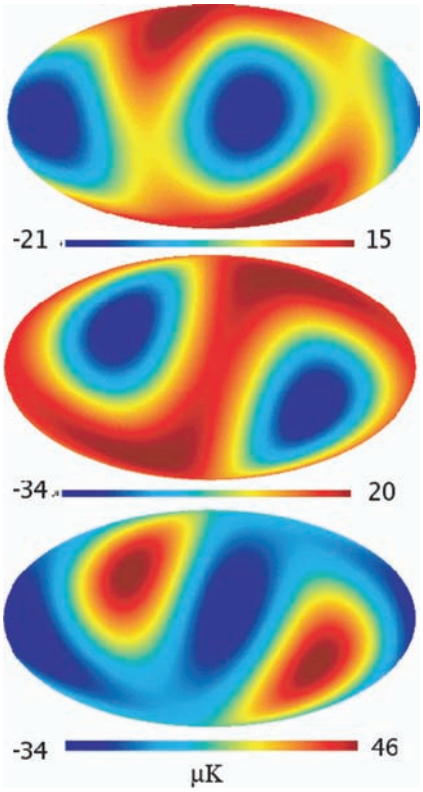

Figure 9. From top to bottom: *WMAP* 5-year quadrupole (Q_{WMAP}), quadrupole of the hypothetical signal in the ecliptic plane ($Q_{\rm ecl}$) and the difference $Q_{WMAP} - Q_{\rm ecl}$.

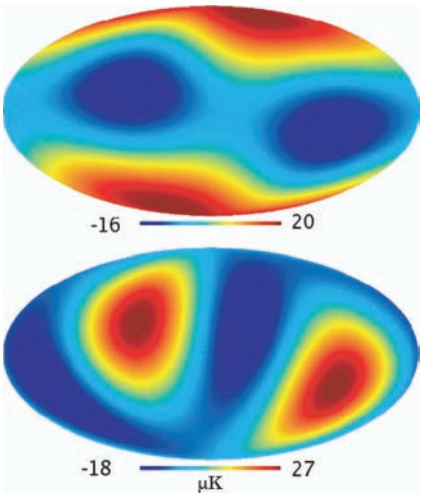

Figure 10. Top: quadrupole of a signal with the same spatial pattern as in Fig. 1 and a flux going as ν^2. Bottom: difference of *WMAP* (ILC) quadrupole and the quadrupole in the top panel.

second toy model follows the spatial distribution of the residual (Fig. 1). We adopt a similar approach to the one described above. We assume a frequency dependence for the signal to ν^2 and set the normalization such that the amplitude of $V + W - 2Q$ is about 10 μK. This model predicts an ILC amplitude of about 55 μK, again subdominant when compared when the amplitude of the ILC from the CMB. The corresponding quadrupole is shown in Fig. 10 together with the difference of the measured quadrupole minus the quadrupole from our toy model. The amplitude of the quadrupole is not as large with the second toy model, but it still impacts the measured quadrupole in a way similar to the toy model by reducing its amplitude and especially changing its orientation. Moreover, the quadrupole from the second toy model is also anticorrelated with the measured quadrupole.

In this paper, we have assumed a simple model for the ZLE. A detailed discussion of phenomenological and physical models for the ZLE involving modifications of geometrical assumptions and grain emission properties is the object of a future work. Regarding geometry, both deviations from almost exact azimuthal symmetry of the interplanetary dust cloud and variation in the scaleheight could be investigated while different assumptions on grain temperature and size imply a spectral shape different from that adopted in this investigation.

8 DISCUSSION AND CONCLUSIONS

Our analysis of the large-scale residuals in the combination map $V + W - 2Q$ reveals a signal which is inconsistent with the expected instrumental noise. This signal could be in principle explained with a variety of spectra ranging from blackbody-like spectra to dust-like spectra. It appears in areas with low Galactic contamination suggesting that is either from extragalactic origin or from our Solar system. Two possible explanations are explored to explain this signal; ZLE and unresolved compact sources (PS). Neither the ZLE nor the PS alone seems to be able to explain the magnitude of the observed high Galactic latitude signals. However, the models considered in this work are not very well constrained, hence significant variations in the expected intensity of the ZLE and PS are still possible. In the case of the ZLE, a hypothetical, yet undetected, cold dusty component (with $\alpha \approx 0$) could significantly boost the

flux at *WMAP* frequencies when compared with the extrapolations performed from higher frequencies. We investigate alternative explanations like residual emission from the Galaxy and the Sunyaev–Zel'dovich effect but these possibilities are not able to explain in a convincing way the redder zones. However, a combination of the effects is still possible in order to explain at least the redder zone near the Virgo region. The southern redder zone is harder to explain as there is no super-bright cluster (like Virgo) in this region. This issue will need to be resolved with future data, in particular with Planck data which will cover a wider range of frequencies. Finally, we investigate the possible impact of the non-removed ZLE and PS in the determination of the quadrupole and octupole in *WMAP* data. Our results show that the measurements of the quadrupole and octupole should not be affected by the non-removed ZLE or PS. However, alternative models with a quasi-blackbody spectrum could explain both the redder zones and the low-ℓ anomalies previously detected in the *WMAP* data. We explore two toy models. The first has the same spatial distribution of the ZLE and the second has the same spatial distribution of the residual in the combination $V + W - 2Q$. Both models predict a significant reduction in the observed amplitude of the quadrupole and in its orientation. Simultaneously with this work, Jiang, Lieu & Zhang (2009) made an independent analysis similar to the one presented here but focusing on the smallest scales (i.e. without applying any Gaussian smoothing to the data). In that paper, the authors found a spectral dependency in the residual of the difference *WMAP* bands which is consistent with our findings.

ACKNOWLEDGMENTS

The authors would like to thank Richard Lieu, Bizhu Jiang, Hiranya Peiris and Andrew Pontzen for interesting discussion and comments. JMD benefits from a Ministerio de Educación y Ciencia "Ramón y Cajal" contract. JMD and MC also acknowledge support from the Ministerio de Educación y Ciencia project AYA2007-68058-C03-02. YA acknowledges support from the Ministerio de Educación y Ciencia project AYA2007-67965-C03-03. Partial financial support for this research has been provided to JGN, MM and CB by the Italian ASI (contracts Planck LFI Activity of Phase E2 and de ASI contract I/016/07/0 COFIS) and MUR. Some of the results in this paper have been derived using the HEALPIX (Gorski et al. 2005) package. We would like to thank the *WMAP* team for making the data available to the community.

REFERENCES

Abramo L. R., Sodré L., Jr., Wuensche C. A., 2006, Phys. Rev. D, 74, 083515
Beichman C. A., Neugebauer G., Habing H. J., Clegg P. E., Chester T. J., eds., 1988, Infrared Astronomical Satellite (IRAS) Catalogs and Atlases, Vol. 1, Explanatory Supplement, NASA RP-1190. GPO, Washington, DC
Bennett C. L. et al., 2003, ApJS, 148, 97
Bielby R. M., Shanks T., 2007, MNRAS, 384, 1196
Blake C.., Wall J., 2002, MNRAS, 329, L37
Bunn E. F., Bourdon A., 2008, Phys. Rev. D, 78, 123509
Condon J. J., Cotton W. D., Greisen E. W., Yin Q. F., Perley R. A., Taylor G. B., Broderick J. J., 1998, AJ, 115, 1693
Copi C. J., Huterer D., Schwarz D. J., Starkman G. D., 2006, MNRAS, 367, 79
de Oliveira-Costa A., Tegmark M., 2006, Phys. Rev. D, 74, 3005
Diego J. M., Ascasibar Y., 2008, MNRAS, 389, 1805
Diego J. M., Martínez-González E., Sanz J. L., Benitez N., Silk J., 2002, MNRAS, 331, 556
Dobler G., Finkbeiner D. P., 2008, ApJ, 680, 1222
Dolag K., Hansen F. K., Roncarelli M., Moscardini L., 2005, MNRAS, 363, 29
Dunlop J. S.., Peacock J. A., 1990, MNRAS, 247, 19
Dunne L., Eabes S., Edmunds M., Ivison R., Alexander P., Clements D. L., 2000, MNRAS, 315, 115
Fixsen D. J., Dwek E., 2002, ApJ, 578, 1009
Finkbeiner D. P., 2004, ApJ, 614, 186
Fomalont E. B., Windhorst R. A., Kristian J. A., Kellerman K. I., 1991, AJ, 102, 1258
González-Nuevo J., Toffolatti L., Argüeso F., 2005, ApJ, 621, 1
Gorski K. M., Hivon E., Banday A. J., Wandelt B. D., Hansen F. K., Reinecke M., Bartelmann M., 2005, ApJ., 622, 759
Gregory P. C., Scott W. K., Douglas K., Condon J. J., 1996, ApJS, 103, 427
Gregory P. C., Vavasour J. D., Scott W. K., Condon J. J., 1994, ApJS, 90, 173
Hauser M. G. et al., 1997, in Hauser M. G., Kelsall T., Leisawitz D., Weiland J., eds, COBE Diffuse Infrared Background Experiment (DIRBE) Explanatory Supplement 1997 COBE Ref. Pub. Mo. 97-A. NASA GSFC, Greenbelt, MD (http://www.gsfc.nasa.gov/astro/cobe/cobe_home.html)
Hinshaw G., Banday A. J., Bennett C. L., Gorski K. M., Kogut A., Smoot G. F., Wright E. L., 1996, ApJ, 464, 17
Hinshaw G. et al., 2007, ApJS, 170, 288
Hinshaw et al., 2009, ApJS, 180, 225
Jiang B.-Z., Lieu R., Zhang S.-N. 2009, ApJ, submitted (arXiv0904.2513)
Jones M. H., Rowan-Robinson M., 1993, MNRAS, 264, 237
Kelsall T. et al., 1998, ApJ, 508, 44
Kuehr H., Witzel A., Pauliny-Toth I. I. K., Nauber U., 1981, A&AS, 45, 367
Land K., Magueijo J., 2007, MNRAS, 378, 153.
Leach S. M. et al., 2008, A&A, 491, 597
López-Caniego M., González-Nuevo J., Herranz D., Massardi M., Sanz J. L., De Zotti G., Toffolatti L., Argüeso F., 2007, ApJS, 170, 108
Maris M., Burigana C., Fogliani S., 2006, A&A 452, 685
Massàrdi M. et al., 2008, MNRAS, 384, 775
Mauch T., Murphy T., Buttery H. J., Curran J., Hunstead R. W., Piestrzynski B., Robertson J. G., Sadler E. M., 2003, MNRAS, 342, 1117
Moshir M., Kopman G., Conrow T. A. O., 1992, Pasadena: Infrared Processing and Analysis Center, California Institute of Technology
Negrello M., Perrotta F., González-Nuevo J., Silva L., De Zotti G., Granato G. L., Baccigalupi C., Danese L., 2007, MNRAS, 377, 1557
Ricci R., Prandoni I., Gruppioni C., Sault R., de Zotti G., 2006, A&A, 445, 465
Stickel M., Meisenheimer K., Kuehr H., 1994, A&AS, 105, 211
Sunyaev R. A., Zel'dovich Ya. B., 1972, A&A, 20, 189

This paper has been typeset from a TEX/LATEX file prepared by the author.